

4-25-2024

## Construction of hyperbranched imprinted nanomaterials for selective adsorption of cadmium (II)

SHENG NAN HU

XINYU ZHANG

MING GUO

SHENGCHUN WU

WENJUN LU

Follow this and additional works at: <https://journals.tubitak.gov.tr/chem>

 Part of the [Chemistry Commons](#)

### Recommended Citation

HU, SHENG NAN; ZHANG, XINYU; GUO, MING; WU, SHENGCHUN; and LU, WENJUN (2024) "Construction of hyperbranched imprinted nanomaterials for selective adsorption of cadmium (II)," *Turkish Journal of Chemistry*. Vol. 48: No. 2, Article 14. <https://doi.org/10.55730/1300-0527.3664>  
Available at: <https://journals.tubitak.gov.tr/chem/vol48/iss2/14>

This Article is brought to you for free and open access by TÜBİTAK Academic Journals. It has been accepted for inclusion in Turkish Journal of Chemistry by an authorized editor of TÜBİTAK Academic Journals. For more information, please contact [pinar.dundar@tubitak.gov.tr](mailto:pinar.dundar@tubitak.gov.tr).

## Construction of hyperbranched imprinted nanomaterials for selective adsorption of cadmium (II)

Sheng Nan HU<sup>1</sup>, Xinyu ZHANG<sup>1</sup>, Ming GUO<sup>1\*</sup>, Shengchun WU<sup>2</sup>, Wenjun LU<sup>1</sup>

<sup>1</sup>Department of Chemistry and Materials Engineering, Zhejiang Agriculture & Forestry University, Hangzhou, China

<sup>2</sup>Department of Environmental and Resource Sciences, Zhejiang Agriculture & Forestry University, Hangzhou, China

Received: 07.10.2023 • Accepted/Published Online: 20.02.2024 • Final Version: 25.04.2024

**Abstract:** A hyperbranched ion-imprinted polymer (IIP) material containing multiple selective adsorption sites was synthesized using halloysite nanotubes, methyl acrylate, and ethylenediamine in the presence of a template ion [i.e. Cd (II) heavy metal]. The successful preparation of the Cd-IIP composition was confirmed by FT-IR, XRD, TEM, TGA, and elemental analysis. The polymers exhibited good adsorption of Cd (II) with a maximum adsorption capacity of 64.37 mg·g<sup>-1</sup>. The imprinting factor ( $\alpha$ ) for Cd (II) was 2.62 and the selection factor ( $\beta$ ) was 1.78, indicating a specific adsorption of Cd (II) ion. The selection coefficients of Cd-IIP for Cd (II)/Pb (II), Cd (II)/Cu (II), Cd (II)/Ni (II), Cd (II)/Cr (III), and Cd (II)/Na (I) also indicated an excellent selectivity of the hyperbranched polymers for Cd (II) in the presence of competitive ions. The removal efficiency remained more than 75% after five cycles of desorption/adsorption. We envision that the HNTs based Cd-IIP has promising applications in the removal of Cd (II) from wastewater.

**Keywords:** Halloysite, ion-imprinting, hyperbranched polymer, cadmium ion, specific adsorption

### 1. Introduction

Heavy metal ions are the major pollutants in wastewater [1,2]. The extensive heavy metal pollution of water resources caused by man-made or natural sources threatens access to clean drinking water globally [3]. In addition, exposure to low concentrations of these metal contaminants may cause cardiovascular, immune, neurological, and endocrine disorders, and cancers [4]. Many technologies have been developed to remove the metal ions from wastewater, such as ion exchange, filtration, solvent extraction, and sorption [5–11]. In particular, sorption is a facile and effective method due to its cost-effectiveness, versatility, and simplicity in removing trace-level of metal ions from aqueous systems [12].

Nanomaterial-based adsorbents have attracted paramount interest in the removal of metal ions due to the large surface areas, ease of modification, and multiple adsorption sites [13]. Nonetheless, a good separation of contaminants along with a remarkable reusability is still challenging for current nano-adsorbents. Furthermore, the residual nanomaterials in water may cause secondary pollution. Therefore, alternative adsorbents of excellent separation and regeneration properties are highly desirable.

The ion imprinting technique uses the target ion as a template for cross-linking polymerization, and the pores formed by the resulting polymer are specific, and the pore properties are related to the structure and size of the target ion [14–17]. For example, Zhang et al. [18] synthesized a novel N-doped carbon nanotube decorated with fish-scale molybdenum disulfide nanosheets (C-PPy@MoS<sub>2</sub>) by high-temperature hydrothermal reaction, which exhibited a maximum Pb (II) removal capacity of 381.87 mg·g<sup>-1</sup>. Guo et al. [19] designed and synthesized ZnNiCr layered double hydroxides for the removal of hexavalent chromium by microwave hydrothermal method with a maximum adsorption capacity of 28.2 mg·g<sup>-1</sup>. However, most ion-imprinted polymers still have the problems of low active site density, slow target-binding rates, low adsorption saturation, and poor specificity [20]. Specifically, the polymerization reaction causes the imprinted sites to be encapsulated, which is not conducive to adsorption [21]. Mehdinia et al. [22] prepared surface imprinted polymers of cadmium ions on amino-modified silane surfaces using graft polymerization reaction, a saturation adsorption capacity of 36.30 mg·g<sup>-1</sup> for Cd (II). The grafted imprinted polymer increases the density and adsorption capacity of the active site and improves the defects of the polymerization reaction.

\* Correspondence: guoming@zafu.edu.cn

Halloysite nanotubes (HNTs) are nanomaterials discovered in recent years [23–27]. They feature in a hollow tubular structure, abundant interfacial hydroxyl groups, and high porosity. In addition, surface-modified HNTs are cost-effective, stable, and environmental-friendly carriers. Separately, the hyperbranched polymer forms a three-dimensional network structure and shows great potential for adsorption applications due to the multiple adsorption sites [28]. The combination of HNTs and hyperbranched polymers can achieve synergistic effect and enhance the removal efficiency of Cd (II). Heavy metal adsorbents satisfying the advantages of green, cheap and high adsorption capacity were prepared. Therefore, we hypothesized that the application of HNTs and hyperbranched polymers to the development of ion-imprinted materials could overcome the problems of low adsorption capacity and poor specificity faced by most current ion-imprinted materials.

In this study, we grafted the hyperbranched polymers onto the HNTs by surface imprinting polymerization [i.e. Cd (II)-imprinted polymers] for specific Cd (II) ion removal [29]. HNTs were used as the starting materials, and a dispersed synthesis route was used to introduce hyperbranched terminal amino groups on the surface [30]. The large number of imprinting sites were provided by the hyperbranched polymers, thus increasing the saturated adsorption capacity of target ions. Our heavy metal adsorbent is easy to prepare, inexpensive, highly specific, and has a large adsorption capacity compared with the traditional ion-imprinted polymers. In addition, the results showed that the polymer HNTs adsorbent retained 75% of Cd (II) removal after five desorption-adsorption cycles.

## 2. Experimental

### 2.1. Materials

Halloysites (HNTs) were purchased from Hebei Qingtai Mineral Products Co., Ltd. Ethyl ether, methanol, anhydrous ethylenediamine (EDA), cadmium nitrate, lead nitrate and chromium nitrate were purchased from Saen Chemical Technology Co., Ltd. Methyl acrylate (MA), 3-aminopropyltriethoxysilane (APTES), polyacrylamide (PAM), epichlorohydrin (ECH) and azobisisobutyronitrile (AIBN) were purchased from Sinopharm Chemical Reagent Co., Ltd.

### 2.2. Sample preparation

Synthesis of the terminal amino hyperbranched molecule NHNTs-3: To purify and decontaminate HNTs. We stirred 5 g of HNT in hydrochloric acid solution (35%) for 24 h, then washed 3 times with distilled water to obtain the acidified HNTs. The acidified HNTs were added to a mixture of toluene (25 mL) and APTES (7 mL) and reflux at 60 °C for 8 h under N<sub>2</sub> protection. The mixture was then collected using filtration and washed with diethyl ether, ethanol and methanol 5 times for each solvent. The mixture was then dried at 60 °C to obtain amino-modified HNTs (AHNTs). The prepared AHNTs were added to ethanol (20 mL) followed by MA (10 mL). The mixture was stirred at 60 °C for 12 h, filtered and washed 5 times with methanol, then dried at 60 °C to obtain the intermediate MHNTs. Grinding yielded MHNTs that were grafted with MA. The prepared MHNTs and EDA (10 mL) were added to methanol (30 mL). The resulting mixture was stirred at 60 °C for 24 h, washed with methanol 5 times, then dried at 60 °C. Grinding yielded the product NHNTs-1. The process of grafting MA then EDA was repeated to obtain the terminal amino hyperbranched molecules on NHNTs-1 to give the terminal amino hyperbranched molecules NHNTs-2 and NHNTs-3 [31,32].

Synthesis of Halloysite-based ion-imprinted hyperbranched polymer (Cd-IIP): Cd (NO<sub>3</sub>)<sub>2</sub> (20 mL, 0.1 M) was added to an Erlenmeyer flask with methanol (15 mL), NHNTs-3 (2 g) and PAM (1.5 g). After oscillating the mixture at 40 °C for 3 h, and then the cross-linking agent ECH (6.5 g) and initiator AIBN (0.15 g) were added. After uniform stirring, the mixture was heated and oscillated for 6 h at 50 °C in an N<sub>2</sub> atmosphere. The resulting product added to a dilute hydrochloric acid solution (2 M), shaken at 50 °C in a shaker until Cd (II) could not be detected using atomic absorption spectrophotometer (AAS), they were then washed with methanol to neutral. The resulting Cd-IIP was then dried under vacuum at 60 °C. Nonimprinted polymer (NIP) adsorbents were fabricated using the same procedure without the addition of the template ions.

Fourier transform infrared spectroscopy (FTIR, IR Prestige-21, Japan) was used to characterize, this confirmed that the IIP was successfully prepared. Scanning electron microscope and energy spectrometer (SEM-EDS, JSM-7800F, Japan) were used for morphological analysis. Transmission electron microscope (TEM, Tecnai F30G2, United States) were used to analyze the apparent morphology of the sample. The Brunauer-Emmett-Teller (BET, NOVA, United States) method calculates the specific surface area.

The thermal properties of the samples were tested using a thermal analyzer (2090F3, Germany). The grafting rate was calculated from the thermogravimetric (TG) curves. Characterization of sample structure using nuclear magnetic resonance (NMR, Varian Inova-400, United States). The samples to be tested were mixed with deuterated chloroform reagent by sonication and dissolved and transferred to the NMR tube for testing. The data obtained were analyzed using MestReNova software.

### 2.3. Adsorption performance experiments

The adsorption and specific recognition of Cd (II) by the HNTs, Cd-IIP and NIP were investigated under different conditions. The amount of imprinted adsorption was calculated using the Lambert-Beer law and the Eq. 1.

$$Q = \frac{(C_0 - C_e) \cdot V}{W} \quad (1)$$

where  $Q$  is the amount of adsorption,  $W$  is the mass of the polymer,  $C_0$  is the initial concentration of the Cd (II), and  $C_e$  is the concentration of the Cd (II) after adsorption equilibrium,  $V$  is the volume of the adsorbent.

Cd ( $\text{NO}_3$ )<sub>2</sub> solutions (20 mL, 100 mg·L<sup>-1</sup>) were added to Erlenmeyer flasks. The ion concentration in the supernatant was determined by AAS. The imprint factor ( $\alpha$ ) and the selection factor ( $\beta$ ) were calculated using Eq. 2, and these were used to analyze the specificity of the different materials for Cd (II) ions.

$$\alpha = Q_{IIP} / Q_{NIP} ; \quad \beta = (Q_{IIP} - Q_{NIP}) / Q_{NIP} \quad (2)$$

where  $Q_{IIP}$  is the amount of adsorption of the substrate by the molecularly imprinted polymer;  $Q_{NIP}$  is the amount of adsorption of the blank control substrate.

$$K_d = \frac{C_p}{C_s} \quad (3)$$

$$k = \frac{K_d(\text{Cd(II)})}{K_d(\text{M})} ; \quad k' = \frac{k_{IIP}}{k_{NIP}} \quad (4)$$

where  $C_p$  is the concentration of the polymer bound substrate, and  $C_s$  is the concentration of the substrate in the solution at adsorption equilibrium;  $K_d$  (Cd (II)),  $K_d$  (M) are the partition coefficients of Cd (II) and reference ions, respectively;  $K_{IIP}$  and  $K_{NIP}$  are the selectivity coefficients of Cd-IIP and NIP.

Pb (II), Cu (II), Ni (II), and Cr (III) were selected competitors for Cd (II) adsorption. Solutions containing Cd (II) ions (100 mg·L<sup>-1</sup>) and the competitor ions were prepared mixed solutions (100 mg·L<sup>-1</sup>). HNTs, Cd-IIP or NIP (20 mg) were added to the mixed solutions (20 mL) and shaken at 25 °C for 180 min. The concentration of metal ions in the solution was determined by AAS. The partition coefficient of NIP for each ion was calculated according to Eq. 3. Eq. 4 was used to calculate the selectivity coefficient ( $k$ ) and the relative selectivity coefficient ( $k'$ ).

## 3. Results and discussion

Cd-IIP (Hyperbranched ion-imprinted polymers based on HNTs), NHNTs-1 (1st generation), NHNTs-2 (2nd generation) and NHNTs-3 (3rd generation) were prepared according to the reaction route (Figure 1). The silane coupling agent APTES (i.e. HNTs with silanol structures after APTES catalysis) was chemically bonded to the surface of the HNTs to prepare the amino functionalized AHNTs. These amine groups underwent Michael addition to the double bond in MA and yielded the MA-modified MHNTs. The use of EDA allowed two amino groups to be grafted on MHNTs by amidation reaction and produced the NHNTs-1, which was sequentially reacted with MA and EDA to prepare the hyperbranched NHNTs-2 and NHNTs-3 structures. Then, by the surface ion-imprinting technique, using PAM as the functional monomer, Cd (II) as the template ion, and NHNTs-3 as the imprinted substrate, a complex was formed. The crosslinking agent ECH was added to the complex and prepared by crosslinking and polymerization with PAM in the presence of an initiator AIBN to obtain the ion-imprinted polymer (IIP). Finally, the template was eluted under acidic conditions and the hyperbranched ion-imprinted polymer with specific selective recognition to Cd (II) (Cd-IIP) was obtained.

### 3.1. Structural characterization of ion-imprinted polymer Cd-IIP

The results of FTIR spectra analysis show that the characteristic peaks of Al-O stretching vibrations (from the inner surface of the HNTs) were observed at 3623 and 3693 cm<sup>-1</sup> (Figure 2a), while the bending vibrations from an intermediate layer of water on the HNTs were observed at 1635 cm<sup>-1</sup>. The peak at 915 cm<sup>-1</sup> denotes the O-H bending vibration on the HNTs surface, and characteristic peaks of bending vibrations from Si-O, Al-O-Si and Si-O-Si were observed at 1036, 534, and 482 cm<sup>-1</sup>, respectively. The AHNTs retained the original absorption peaks that were observed from the HNTs (Figure 2b). At the same time, the N-H stretching vibration peak appeared at 3448 and 1561 cm<sup>-1</sup>, and C-H vibration peak appeared at 2934, 2873, and 1482 cm<sup>-1</sup> [33,34].

The FTIR spectrum of the MHNTs exhibited a peak (1731 cm<sup>-1</sup>) from a carbonyl group, implying that the grafting of EDA was also successful (Figure 2c). The presence of N-H stretching and bending vibrations and the increased peak area of NHNTs-1 (Figure 2d), NHNTs-2 (Figure 2e), and NHNTs-3 (Figure 2f) indicate a higher generation of amination. Cd-IIP

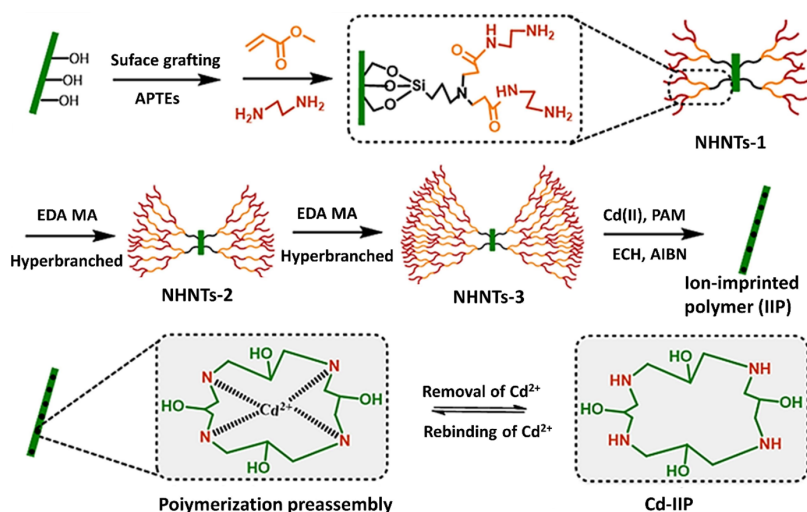


**Figure 1.** The synthetic route of hyperbranched ion-imprinted polymer (Cd-IIP) and 3rd generation amino-hyper hybridization.

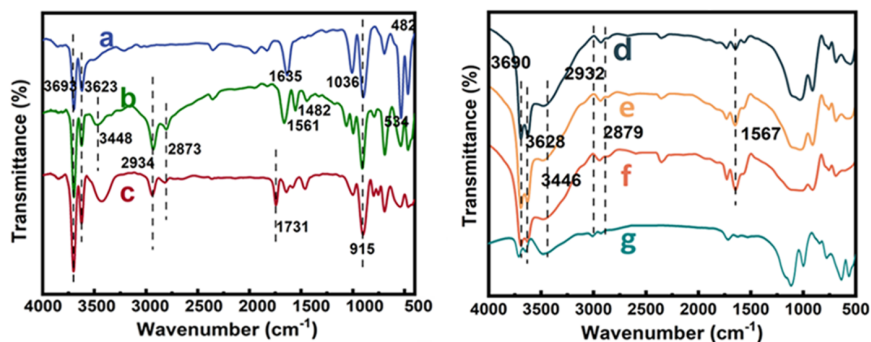


**Figure 2.** FT-IR spectra of HNTs (a), AHNTs (b), MHNTs (c), NHNTs-1(d), NHNTs-2 (e), NHNTs-3 (f), and Cd-IIP (g).

(Figure 2g) exhibited strong hydroxyl peak at 3450 and 1636  $\text{cm}^{-1}$  compared to the FTIR spectrum of NHNTs-3 (Figure 2f), indicating that a ring-opening reaction occurred on the cross-linking agent epichlorohydrin. This indicates that the cross-linker was involved in the synthesis and the Cd-IIP, which laterally proves that Cd-IIP was successfully prepared. The peaks at 1084 and 542  $\text{cm}^{-1}$  were characteristics of stretching vibration of Cd (II)-N, which confirmed that Cd (II) was successfully doped to the active sites. All the above analyses confirmed that the Cd-IIP was successfully synthesized.

The results of  $^1\text{H}$  NMR spectrum analysis show that NHNTs-1 is the first generation of hyperbranched polymers with a simple molecular structure (Figure 3a). The resonance peaks of the  $-\text{CH}_2-$  groups on the main chains of NHNTs-1 and NHNTs-3 were observed at  $\delta = 4.0$  ppm and  $\delta = 4.1$  ppm, respectively. In the main chains of NHNTs-1 and NHNTs-3, characteristic peaks of  $-\text{NH}_2$  were observed at  $\delta = 1.4$  ppm and  $\delta = 1.6$  ppm [35]. The integration region of NHNTs-3 widened, and the chemical shift is changed. This is probably due to the growing number of amino groups as the number of hyperbranched generations increases and the absorption band becomes wider. The peaks at  $\delta = 4.1$  ppm and  $\delta = 1.6$  ppm in the spectra are broad, with a slight change in the peak height. This is mainly due to the increasing degree of terminal amino substitution.

X-ray diffraction (XRD) analysis. The standard card of HNTs showed significant diffraction peaks at (NO.29-1487) at  $2\theta$  of 12.09°, 20.06°, 24.52°, 35.12°, 55.62°, and 63.59°. The characteristic diffraction peaks belonging to HNTs nanotubes are still present in the X-ray diffraction spectra of the structurally modified HNTs, NHNTs-3, and Cd-IIP (Figure 3b), but the magnitude of the diffraction peak intensity has changed, which indicating that the basic structure is not destroyed. The hyperbranched macromolecules on the surface modification of nanotubes existed in the amorphous form, which did not significantly affect the overall crystal structure of the products.

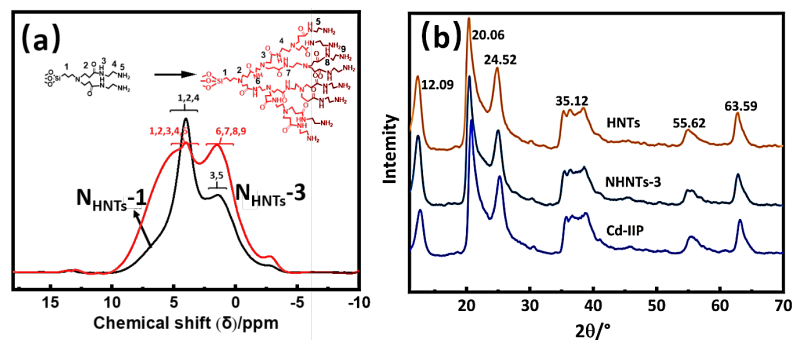


**Figure 3.**  $^1\text{H}$  NMR spectrum of NHNTs-1 and NHNTs-3 (a), XRD diagram of HNTs, NHNTs-3, and Cd-IIP (b).

The EDS spectroscopy of HNTs and AHNTs shows (Figures 4a and 4b) that the nitrogen content increased from that the nitrogen content increased from 1.68% to 2.92% after the silane coupling process, while the oxygen content decreased from 44.97% to 33.80%, indicating that the APTES successfully reacted with the HNTs. As can be seen from Figures 4c–4e, the elemental N contents were 3.69%, 5.06%, and 6.97%, respectively, with a significant increasing trend of N content. The successful modification of supramolecular groups containing amino terminals on NHTs was confirmed. The carbon content increased from 20.54% to 25.55%, and the oxygen content increased from 40.48% to 44.04% (Figures 4e and 4f), confirming that the Cd-IIP was successfully prepared. The presence of traces of Cd in the EDS of Cd-IIP (Figure 4f) is caused by traces of Cd(II) ions remaining after the elution process.

The results of TEM analysis show that the HNTs are hollow and transparent cylindrical nanotubes (Figure 5a). They are open at both ends, double-layered, and have a smooth surface. Cd-IIP (Figure 5b) and NIP (Figure 5c) had a bilayer and tubular morphology, which was significantly rougher than that of the HNTs. Although the surface of the NIP is irregular and flat, the surface of the Cd-IIP is rough, uneven, and porous. A comparison of the TEM images shows that the surface of NIP is rough and uneven with a loose and porous surface. This may be caused by the imprinted holes that remained after the template ions were eluted, which indicates that the target product was obtained.

The surface areas of HNTs, Cd-IIP and NIP were tested according to BET analysis by nitrogen adsorption, and the tested surface areas were 37.69, 76.96 and 42.1  $\text{m}^2\cdot\text{g}^{-1}$ , respectively [36]. It is clear from Table 1 that the total specific surface area and pore capacity of HNTs increased after modification, which indicates that the material preparation is consistent with the expectation [37]. It is that the specific surface area and pore capacity of NIP are smaller than those of Cd-IIP, but the average pore size of NIP is larger, which explains the formation of imprinted cavities of Cd-IIP [38].

TGA plots of HNTs, AHNTs, NHNTs-3 and Cd-IIP showed (Figure 6) that all materials exhibited weight loss in the range of 0–150  $^{\circ}\text{C}$ , mainly due to the loss of adsorbed water. HNTs showed no significant weight loss at 700  $^{\circ}\text{C}$ , indicating that the thermal stability of the support is good. However, NHNTs-3 showed weight loss from 100–600  $^{\circ}\text{C}$ , which may be caused by the dehydrogenation of Al-OH. The weight loss of Cd-IIP from 250–600  $^{\circ}\text{C}$  was greater than that of NHNTs-3. This may be due to the increase in the content of pyrolytic components after the formation of imprinted polymers. The surface grafting of HNTs was successful by calculating the grafting rate (Table 2) by TG analysis.

### 3.2. Adsorption of Cd (II) ions by Cd-IIP

The amount of Cd (II) that was adsorbed by Cd-IIP and NIP was calculated, and the adsorption isotherm was plotted (Figure 7). The amount of Cd (II) adsorbed by Cd-IIP and NIP increased with increasing substrate concentration. The saturated adsorption capacities of Cd-IIP and NIP are 64.37 and 34.8  $\text{mg}\cdot\text{g}^{-1}$ , respectively. The isothermal adsorption equations of the two materials showed a good linear correlation.

Freundlich and Langmuir adsorption isotherm models (Eqs 5 and 6) were used to fit the data, and the kinetic adsorption curves (Figures 8a and 8b) were obtained [39,40].

$$\ln q_e = \ln K_F + \frac{1}{n} \ln C_e' \quad (5)$$

$$\frac{C_e'}{q_e} = \frac{C_e'}{q_{\max}} + \frac{1}{q_{\max} K_L} \quad (6)$$

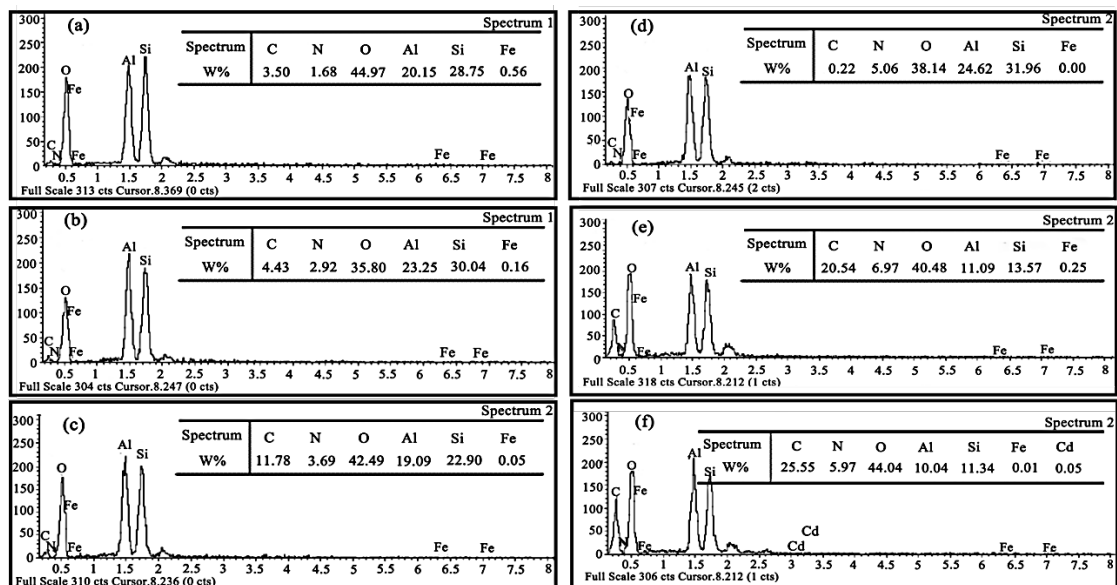


Figure 4. The EDS of HNTs (a), AHNTs (b), NHNTs-1 (c), NHNTs-2 (d), NHNTs-3(e), and Cd-IIP(f).

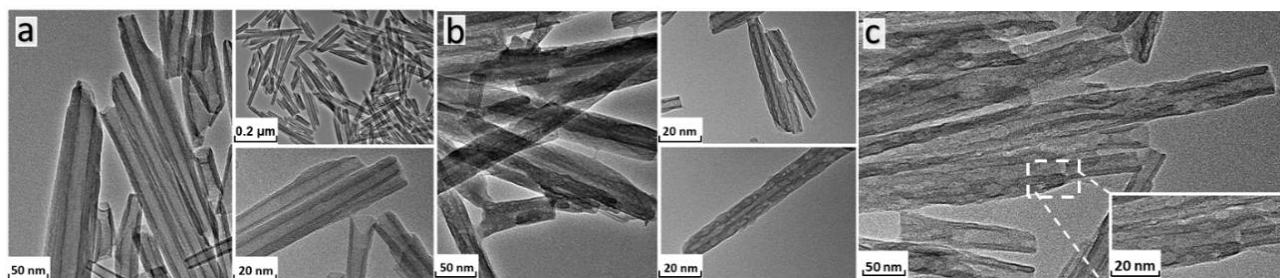


Figure 5. The TEM of HNTs (a), Cd-IIP (b), and NIP (c).

Table 1. Physical properties of hyperbranched ion-imprinted polymers.

Samples	$S_{BET}$ ( $m^2 \cdot g^{-1}$ )	Average pore size (nm)	Pore volume ( $cm^3 \cdot g^{-1}$ )
HNTs	37.69	20.41	0.28
Cd-IIP	76.96	11.28	0.43
NIP	42.10	22.68	0.31

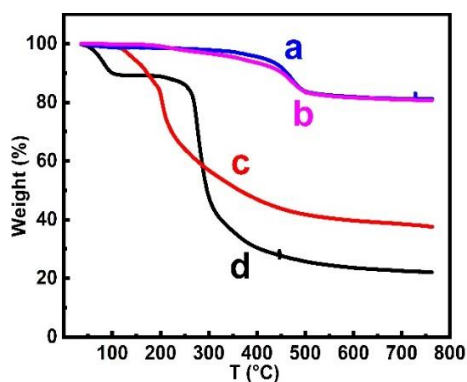
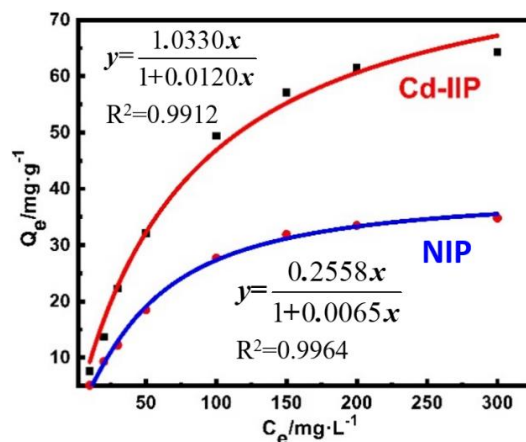


Figure 6. TG diagram of HNTs (a), AHNTs (b), NHNTs-3 (c), and Cd-IIP (d).

**Table 2.** The grafting rate of AHNTs, NHNTs-3, and Cd-IIP.

Samples	Grafting ratio /%	
	Experimental value	Theoretical value
AHNTs	5	15
NHNTs-3	143	163
Cd-IIP	406	422



**Figure 7.** Isotherm adsorption curve of Cd-IIP and NIP.

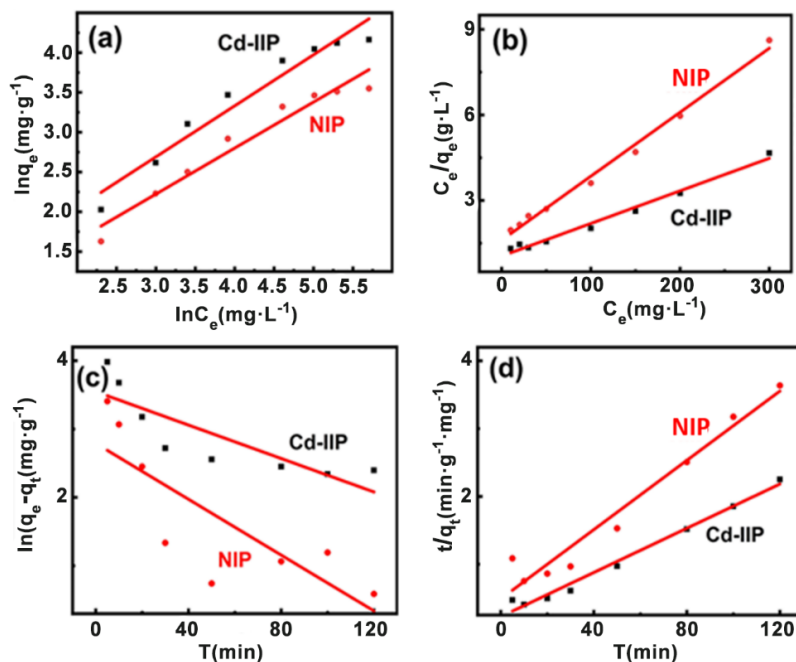


**Figure 8.** Freundlich isotherm adsorption (a), and Langmuir isotherm adsorption (b) model fitting curve, Quasi-first-order (c), and Quasi-second-order (d) dynamics curve.

where  $C_e$  is the ion concentration at equilibrium,  $q_e$  and  $q_{max}$  are the adsorption capacity at equilibrium and saturation, respectively,  $K_F$  and  $K_L$  are the adsorption constants of Freundlich and Langmuir, respectively.

The linear fitting results using the Langmuir model indicated that the maximum adsorption capacities of the two are 62.6 and 33.1  $\text{mg}\cdot\text{g}^{-1}$ , respectively (Table S1), which was more similar to the actual adsorption saturation capacity. Additionally, the  $R^2$  values of the linear correlations using the Langmuir model are greater than 0.98, which is higher than



those obtained by the Freundlich model. Therefore, the Langmuir adsorption isotherm model is more appropriate for modeling the thermodynamic adsorption behavior of Cd-IIP. This indicates that the distribution of active sites is more uniform, the adsorbent is a single molecule adsorption. The maximum adsorption capacity of Cd-IIP for Cd (II) shows that the ion-imprinted polymer had a strong recognition ability for the substrate.

Quasi-first-order and quasi-second-order kinetic models (Figures 8c and 8d) were used to fit the plots. Kinetic adsorption curves for the samples (Figure 9) were plotted.

First order dynamics

$$\ln(q_e - q_t) = \ln q_e - K_1 t \quad (7)$$

Secondary dynamics

$$\frac{t}{q_t} = \frac{1}{K_2 q_e^2} + \frac{t}{q_e} \quad (8)$$

where  $t$  is the adsorption time;  $q_e$  and  $q_t$  are the adsorption amount of the adsorbed material to heavy metals when the adsorption reaches equilibrium; respectively, and  $K_1$  and  $K_2$  are the first and second adsorption rate constants.

The maximum saturation sorption amounts for Cd-IIP and NIP were 54.26 and 33.81  $\text{mg}\cdot\text{g}^{-1}$ , respectively, with Cd-IIP far exceeding NIP. The results of the linear fit of the quasi-primary adsorption kinetic model gave a maximum adsorption of 34.75 and 16.29  $\text{mg}\cdot\text{g}^{-1}$  respectively, while the results of the linear fit of the quasi-secondary adsorption kinetic model gave 56.31 and 37.15  $\text{mg}\cdot\text{g}^{-1}$  respectively. It is noticeable that the equilibrium sorption amounts from the linear fit of the quasi-secondary sorption kinetic model are closer to the measured values and better reflect the kinetic behavior of the material for Cd (II) sorption.

The adsorption capacity of Cd-IIP is greater than that of NIP and HNTs, this is because in Cd-IIP, there are not only binding sites with template molecules, but also imprinted holes that are consistent with the stereoscopic structure of Cd (II). In NIP and HNTs, there are no imprinted holes that are complementary to Cd (II), and there are no sites that have specific adsorption capacity with Cd (II).

### 3.3. Adsorption selectivity of IIP

The adsorption selectivity results can be seen (Figure 10a) in that the adsorption capacity of Cd-IIP is greater than that of NIP and HNTs. The blotting factor  $\alpha$  and the selection factor  $\beta$  were calculated by Eq. 3. The Cd-IIP has an imprinting factor ( $\alpha$ ) of 2.62 for Cd and a selection factor ( $\beta$ ) of 1.78, there was no significant difference between Cu (II) and Pb (II) in  $\alpha$  and  $\beta$ , indicating that Cd-IIP had good specificity for Cd (II).

The ion selection performance parameters of the Cd-IIP are given in Table S2. The Cd-IIP exhibited selection coefficients for Cd (II)/Pb (II), Cd (II)/Cu (II), Cd (II)/Ni (II), Cd (II)/Cr (III), Cd (II)/Na (I), Cd (II)/ $\text{NO}_3^-$  of 2.96, 1.80, 4.50, 4.57, 1.63, and 4.24 respectively, showing excellent selection performance for Cd(II). The larger the number, the better the selectivity of Cd-IIP for the ion. In the presence of competitive ions, the Cd-IIP exhibited excellent selectivity for Cd (II). In the presence of  $\text{NO}_3^-$  and Na (I), Cd-IIP still showed excellent selectivity for Cd (II), however, due to the competition between cations, the selectivity decreased when Na (I) was present.

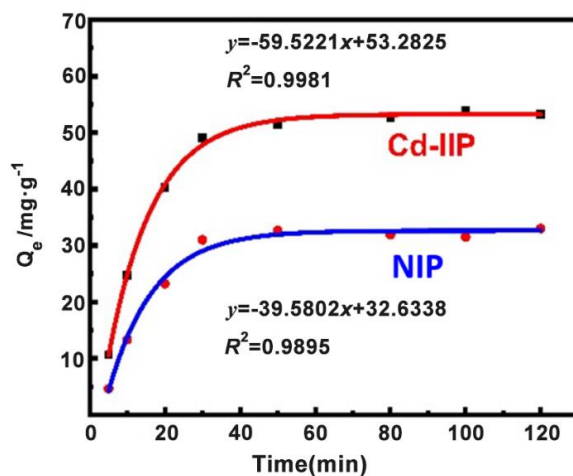
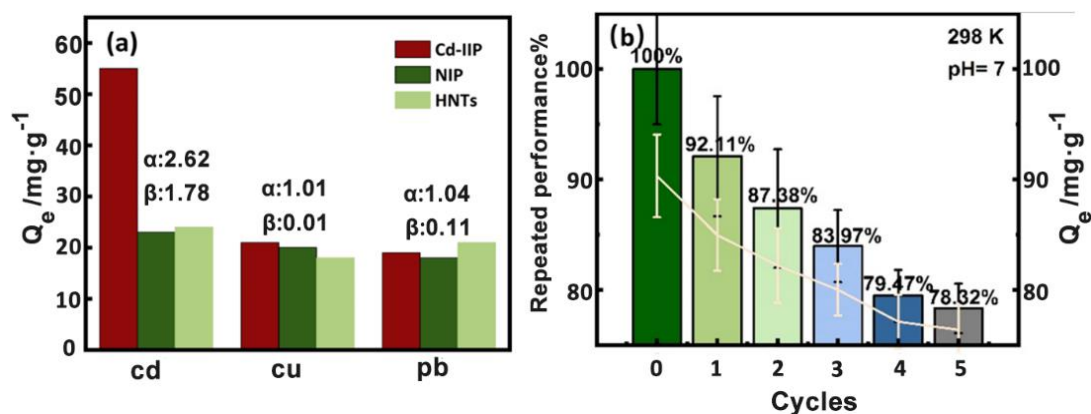


Figure 9. Adsorption kinetic curve of Cd-IIP and NIP.



**Figure 10.** Selective adsorption effect of Cd-IIP, NIP, and HNTs on ions (a), performance of the ion-imprinted polymer Cd-IIP after 5 repeated adsorptions (b).

The adsorption-desorption experiments were repeated five times, and the recovery rate was determined as shown in Figure 10b [41]. After five cycles, the removal rate remained above 75%, the concentration of Cd (II) was  $0.125 \text{ mg}\cdot\text{L}^{-1}$ , highlighting the good regeneration performance of the Cd-IIP. At present, it is stipulated in China that the maximum allowable concentration of Cd (II) in sewage solution should be less than  $0.5 \text{ mg}\cdot\text{L}^{-1}$ , and the maximum allowable concentration in domestic water is  $0.005 \text{ mg}\cdot\text{L}^{-1}$  [42]. Through adsorption experiments and data analysis, it can be known that imprinted polymers have higher saturated adsorption capacity, better selection and recognition performance, and recycling performance.

#### 4. Conclusion

In this study, a hyperbranched ion-imprinted polymer (Cd-IIP) based on HNTs was well-designed and prepared via a surface-ion-imprinted polymerization method. The Cd-IIP is easily regenerated and reused, and it was used for the adsorption of Cd (II) from an aqueous solution. The results showed that the adsorption data fit well with the quasi-secondary kinetics and Langmuir isotherm model, and the maximum adsorption capacity was  $64.37 \text{ mg}\cdot\text{g}^{-1}$ . Previously, Solic et al. [43] applied oxidized multi-walled carbon nanotubes (oxMWCNTs) as an effective adsorbent for the removal of Cd (II) from aqueous medium, and the adsorption equilibrium was reached within 20 min, with a maximum adsorption saturation of  $13.50 \text{ mg}\cdot\text{g}^{-1}$ . Alregeb et al. [44] successfully synthesized hyper-branched polyester nanoparticles by interfacial polymerization, and the adsorption amount of Cd (II) was  $38.9 \text{ mg}\cdot\text{g}^{-1}$  at  $45^\circ\text{C}$ . Qi et al. [45] synthesized a novel Cd (II) ion-imprinted polymer by native polymerization, which showed a maximum adsorption saturation of  $50.54 \text{ mg}\cdot\text{g}^{-1}$  of Cd (II) in  $\text{pH} = 7$  solution. In contrast, our hyperbranched ion-imprinted polymeric adsorbent Cd-IIP synthesized from HNTs is highly promising for the adsorption of Cd (II) in aqueous solution. In addition, the imprinting factors of 2.62, 1.01, and 1.04, and the selectivity factors of 1.78, 0.01, and 0.11 were determined for the adsorption of Cd (II), Cu (II), and Pb (II) pairs by Cd-IIP, indicating that Cd-IIP exhibited better adsorption performance and specific recognition of Cd (II) pairs. The results proved that Cd-IIP could be a specific adsorbent for Cd (II) solution, this work opens a window to develop high-performance sorbents for the removal of heavy metal ions from wastewater.

#### Acknowledgements

This work was financially supported by the Zhejiang Public Welfare Technology Application Research Project (LGN20B070001).

## References

- [1] Dutta K, De S. Aromatic conjugated polymers for removal of heavy metal ions from wastewater: a short review. *Environmental Science: Water Research & Technology* 2017; 3: 793-805. <https://doi.org/10.1039/c7ew00154a>
- [2] Ng CL, Chow WS, Din ATM, Leh CP, Siengchin S. Crosslinked polymer nanocomposites for wastewater heavy metal adsorption: A review. *Express Polymer Letters* 2023; 17 (6): 580-595. <https://doi.org/10.3144/expresspolymlett.2023.43>
- [3] Sun JF, Mu Q, Kimura H, Murugadoss V, He MX et al. Oxidative degradation of phenols and substituted phenols in the water and atmosphere: a review. *Advanced Composites and Hybrid Materials* 2022; 5: 1-14. <https://doi.org/10.1007/s42114-022-00435-0>
- [4] Guo J, Yang Z, Dong HY, Guan XH, Ren QD et al. Simple combination of oxidants with zero-valent-iron (ZVI) achieved very rapid and highly efficient removal of heavy metals from water. *Water Research* 2016; 88: 671-680. <https://doi.org/10.1016/j.watres.2015.10.045>
- [5] Mazur LP, Pozdniakova TA, Mayer DA, Boaventura RA, Vilar JP. Design of a fixed-bed ion-exchange process for the treatment of rinse waters generated in the galvanization process using *Laminaria hyperborea* as natural cation exchanger. *Water Research* 2016; 90: 354-368. <https://doi.org/10.1016/j.watres.2015.12.027>
- [6] Saravanan A, Yaashikaa PR, Kumar PS, Karishma SP, Thamarai VC et al. Environmental sustainability of toxic arsenic ions removal from wastewater using electrodeionization. *Separation and Purification Technology* 2023; 317. <https://doi.org/10.1016/j.seppur.2023.123897>
- [7] Floris RK, Nijmeijer ER, Cornelissen. Removal of aqueous nC60 fullerene from water by low pressure membrane filtration. *Water Research* 2016; 91: 115-125. <https://doi.org/10.1016/j.watres.2015.10.014>
- [8] Liang Y, Xia M, Yu QH, Li YP, Sui YP et al. Guanidinium-based ionic covalent organic frameworks for capture of uranyl tricarbonate. *Advanced Composites and Hybrid Materials* 2022; 5: 184-194. <https://doi.org/10.1007/s42114-021-00311-3>
- [9] Hu Q, Zhou J, Qiu B, Wang Q, Song G et al. Synergistically improved methane production from anaerobic wastewater treatment by iron/polyaniline composite. *Advanced Composites and Hybrid Materials* 2021; 4: 265-273. <https://doi.org/10.1007/s42114-021-00236-x>
- [10] Lin CL, Liu BY, Pu LY, Sun Y, Xue YL et al. Photocatalytic oxidation removal of fluoride ion in wastewater by g-C<sub>3</sub>N<sub>4</sub>/TiO<sub>2</sub> under simulated visible light. *Advanced Composites and Hybrid Materials* 2021; 4: 339-349. <https://doi.org/10.1007/s42114-021-00228-x>
- [11] Yin CZ, Wang C, Hu Q. Selective removal of As (V) from wastewater with high efficiency by glycine-modified Fe/Zn-layered double hydroxides. *Advanced Composites and Hybrid Materials* 2021; 4: 360-370. <https://doi.org/10.1007/s42114-021-00214-3>
- [12] Zhou GY, Luo JM, Liu CB, Chu L, Ma JH et al. A highly efficient polyampholyte hydrogel sorbent based fixed-bed process for heavy metal removal in actual industrial effluent. *Water Research* 2016; 89: 151-160. <https://doi.org/10.1016/j.watres.2015.11.053>
- [13] Hemmatpour H, Haddadi Asl V, Roghani Mamaqani H. Synthesis of pH-sensitive poly (N,N- dimethylamin oethyl methacrylate) -grafted halloysite nanotubes for adsorption and controlled release of DPH and DS drugs. *Polymer* 2015; 65: 143-153. <https://doi.org/10.1016/j.polymer.2015.03.067>
- [14] Xu Y, Zhao Q, Jiang L, Li Z, Chen Y et al. Selective determination of sulfonamides from environmental water based on magnetic surface molecularly imprinting technology. *Environmental Science And Pollution Research* 2017; 24: 9174-9186. <https://doi.org/10.1007/s11356-017-8581-9>
- [15] Ding SC, Li ZL, Cheng Y, Du CB, Gao JF et al. Enhancing adsorption capacity while maintaining specific recognition performance of mesoporous silica: A novel imprinting strategy with amphiphilic ionic liquid as surfactant. *Nanotechnology* 2018; 29: 117619. <https://doi.org/10.1088/1361-6528/aace10>
- [16] Madikizela LM, Tavengwa NT, Tutu H, Chimuka L. Green aspects in molecular imprinting technology: From design to environmental applications. *Trends in Environmental Analytical Chemistry* 2018; 17: 14-22. <https://doi.org/10.1016/j.teac.2018.01.001>
- [17] Ren ZQ, Zhu XY, Du J, Kong DL, Wang N et al. Facile and green preparation of novel adsorption materials by combining sol-gel with ion imprinting technology for selective removal of Cu (II) ions from aqueous solution. *Applied Surface Science* 2018; 435: 574-584. <https://doi.org/10.1016/j.apsusc.2017.11.059>
- [18] Zhang H, Ding X, Wang S, Huang Y, Zeng XF et al. Heavy metal removal from wastewater by a polypyrrole-derived N-doped carbon nanotube decorated with fish scale-like molybdenum disulfide nanosheets. *Chemical Engineering Science* 2022; 18: 320-328. <https://doi.org/10.30919/es8d649>
- [19] Guo L, Zhang F, Zheng J, Shang Q, Shi J et al. Synthesis and characterization of ZnNiCr-layered double hydroxides with high adsorption activities for Cr (VI). *Advanced Composites and Hybrid Materials* 2021; 4: 819-829. <https://doi.org/10.1007/s42114-021-00260-x>
- [20] Moghaddam HK, Pakizeh M. Experimental study on mercury ions removal from aqueous solution by MnO<sub>2</sub>/CNTs nanocomposite adsorbent. *Journal of Industrial and Engineering Chemistry* 2015; 21: 221-229. <https://doi.org/10.1016/j.jiec.2014.02.028>

- [21] Habiba U, Afifi AM, Salleh A, Ang BC. Chitosan/(polyvinyl alcohol)/zeolite electrospun composite nanofibrous membrane for adsorption of  $\text{Cr}^{6+}$ ,  $\text{Fe}^{3+}$  and  $\text{Ni}^{2+}$ . *Journal of Hazardous Materials* 2017; 322: 182-194. <https://doi.org/10.1016/j.jhazmat.2016.06.028>
- [22] Mehdinia A, Dadkhal S, Kayyal TB, Jabbari A. Design of a surface-immobilized 4-nitrophenol molecularly imprinted polymer via pre-grafting amino functional materials on magnetic nanoparticles. *Journal of Chromatography A* 2021; 1364: 12-19. <https://doi.org/10.1016/j.chroma.2014.08.058>
- [23] Joo Y, Jeon Y, Lee SU, Sim JH, Sohn D. Aggregation and stabilization of carboxylic acid functionalized halloysite nanotubes (HNT-COOH). *Journal of Physical Chemistry A* 2012; 116 (34): 18230–18235. <https://doi.org/10.1021/jp3038945>
- [24] Hebbar RS, Isloor AM, Ananda KA, Ismail F. Fabrication of polydopamine functionalized halloysite nanotube/polyetherimide membranes for heavy metal removal. *Journal of Materials Chemistry A* 2021; 4: 764-774. <https://doi.org/10.1039/c5ta09281g>
- [25] Hillier S, Brydson R, Delbos E, Fraser T, Gray N et al. Correlations among the mineralogical and physical properties of halloysite nanotubes (HNTs). *Clays and Clay Minerals* 2016; 51: 325-350. <https://doi.org/10.1180/claymin.2016.051.3.11>
- [26] Li XY, Yang Q, Ouyang J, Yang HM, Chang S. Chitosan modified halloysite nanotubes as emerging porous microspheres for drug carrier. *Applied Clay Science* 2016; 126: 306-312. <https://doi.org/10.1016/j.clay.2016.03.035>
- [27] Zeng GY, He Y, Zhan YQ, Zhang L, Pan Y et al. Novel polyvinylidene fluoride nanofiltration membrane blended with functionalized halloysite nanotubes for dye and heavy metal ions removal. *Journal of Hazardous Materials* 2016; 60-72. <https://doi.org/10.1016/j.jhazmat.2016.05.049>
- [28] Han WS. Synthesis of  $\text{Cu}/\text{SiO}_2$  core-shell particles using hyperbranched polyester as template and dispersant. *Journal of Electronic Materials* 2017; 46: 4676-4681. <https://doi.org/10.1007/s11664-017-5478-9>
- [29] Zhang XF, Du XZ. Protein surface imprinting technology. *Progress in Chemistry* 2016; 28: 149-162. <https://doi.org/10.7536/pc150719>
- [30] Tsubokawa N, Ichioka H, Hayashi TSatoH, Fujiki K. Grafting of 'dendrimer-like' highly branched polymer onto ultrafine silica surface. *Reactive and Functional Polymers* 1998; 37: 75-82. [https://doi.org/10.1016/s1381-5148\(97\)00139-9](https://doi.org/10.1016/s1381-5148(97)00139-9)
- [31] Gnanou Y, Taton D. Stars and dendrimer-like architectures by the divergent method using controlled radical polymerization. *Macromolecular Symposia* 2001; 174: 333-341. [https://doi.org/10.1002/1521-3900\(200109\)174:1<333::aid-masy333>3.0.co;2-w](https://doi.org/10.1002/1521-3900(200109)174:1<333::aid-masy333>3.0.co;2-w)
- [32] Okazaki M, Murota M, Kawaguchi Y, Tsubokawa N. Curing of epoxy resin by ultrafine silica modified by grafting of hyperbranched polyamidoamine using dendrimer synthesis methodology. *Journal Of Applied Polymer Science* 2001; 80: 573-579. [https://doi.org/10.1002/1097-4628\(20010425\)80:4<573::aid-app1132>3.0.co;2-e](https://doi.org/10.1002/1097-4628(20010425)80:4<573::aid-app1132>3.0.co;2-e)
- [33] Wang Q, Zhang JP, Wang AQ. Alkali activation of halloysite for adsorption and release of ofloxacin. *Applied Surface Science* 2013; 287, 54-61. <https://doi.org/10.1016/j.apsusc.2013.09.057>
- [34] Jin ZC, Du L, Zhang CQ, Sugiyama YY, Wang WT et al. Modification of poly (maleic anhydride) - based polymers with  $\text{H}_2\text{N}$ -R nucleophiles: addition or substitution reaction? *Bioconjugate Chemistry* 2019; 30: 871-880. <https://doi.org/10.1021/acs.bioconjchem.9b00008>
- [35] Liu B, Wang XY, Pang CS, Luo JW, Luo YQ et al. Preparation and antimicrobial property of chitosan oligosaccharide derivative/rectorite nanocomposite. *Carbohydrate Polymers* 2013; 92: 1078-1085. <https://doi.org/10.1016/j.carbpol.2012.10.060>
- [36] Zhai YJ, Yang WY, Xie XB, Sun X, Wan QJ et al.  $\text{Co}_3\text{O}_4$  nanoparticle-dotted hierarchical-assembled carbon nanosheet framework catalysts with the formation/decomposition mechanisms of  $\text{Li}_2\text{O}_2$  for smart lithium-oxygen batteries. *Inorganic Chemistry Frontiers* 2022; 9: 1115-1124. <https://doi.org/10.1039/d1qi01260f>
- [37] Wu NN, Zhao BB, Liu JY, Li YL, Chen YB et al. MOF-derived porous hollow Ni/C composites with optimized impedance matching as lightweight microwave absorption materials. *Advanced Composites and Hybrid Materials* 2021; 4: 707-715. <https://doi.org/10.1007/s42114-021-00307-z>
- [38] Sun JX, Shi LX, Song TT, Sun CY. Flame resistance of cotton fabric finishing with N-hydroxymethylacrylamide spiroposphate. *Advanced Composites and Hybrid Materials* 2021; 4: 1155-1165. <https://doi.org/10.1007/s42114-021-00348-4>
- [39] Baghenejad M, Javaheri F, Moosavi AA. Adsorption isotherms of some heavy metals under conditions of their competitive adsorption onto highly calcareous soils of southern Iran. *Archives of Agronomy and Soil Science* 2016; 62: 1462-1473. <https://doi.org/10.1080/03650340.2016.1147647>
- [40] Kim KC, Yoon TU, Bae YS. Applicability of using  $\text{CO}_2$  adsorption isotherms to determine BET surface areas of microporous materials. *Microporous Mesoporous Mat* 2016; 224: 294-301. <https://doi.org/10.1016/j.micromeso.2016.01.003>
- [41] Li T, Zhang WM, Zhai S, Gao GD, Ding J et al. Efficient removal of nickel (II) from high salinity wastewater by a novel PAA/ZIF-8/PVDF hybrid ultrafiltration membrane. *Water Research* 2018; 143: 87-98. <https://doi.org/10.1016/j.watres.2018.06.031>
- [42] Hassan M, Liu YJ, Naidu R, Du JH, Qi FJ et al. Mesoporous biopolymer architecture enhanced the adsorption and selectivity of aqueous heavy-metal ions. *Advanced Materials* 2021; 6: 15316-15331. <https://doi.org/10.1021/acsomega.1c01642>

- [43] Solic M, Maleti S, Isakovski MK, Niki J, Ronevi S et al. Removing low levels of cd(II) and pb(II) by adsorption on two types of oxidized multiwalled carbon nanotubes. *Journal of Environmental Chemical Engineering* 2021; 105402. <https://doi.org/10.1016/j.jece.2021.105402>
- [44] Alregeb F, Khalili F, Sweileh B, Ali DK. Synthesis and characterization of chelating hyperbranched polyester nanoparticles for Cd (II) ion removal from water. *Molecules* 2022; 27 (12): 3656. <https://doi.org/10.3390/molecules27123656>
- [45] Qi DG, Zhang HW, Zhou ZY, Ren ZQ. Cadmium ion-imprinted polymers for adsorption and detection of cadmium ions. *Journal of Environmental Chemical Engineering* 2023; 11 (5). <https://doi.org/10.1016/j.jece.2023.110804>

Supplementary material

**Table S1.** Isotherm adsorption model fitting parameters and parameters of adsorption dynamic model equation.

Freundlich isotherm adsorption					Langmuir isotherm adsorption				
	$q_e$ (mg·g <sup>-1</sup> )	Equation	n	$K_F$	$R^2$	$q_{max}$ (mg·g <sup>-1</sup> )	Equation	n	$R^2$
Cd-IIP	64.300	$y = 0.6409x + 0.7689$	1.560	2.1570	0.9400	62.600	$y = 0.0114x + 1.0518$	0.010	0.9820
NIP	34.800	$y = 0.5778x + 0.4904$	1.730	1.6330	0.9470	33.100	$y = 0.0224x + 1.6101$	0.013	0.9910
Quasi-first-order dynamics					Quasi-secondary dynamics				
	Equation	$q_{e1}$ (mg·g <sup>-1</sup> )	$K_1$	$R^2$	Equation	$q_{e2}$ (mg·g <sup>-1</sup> )	$K_2$	$R^2$	
Cd-IIP	$y = -0.0120x + 3.5480$	34.7500	0.0120	0.6645	$y = 0.0160x + 0.2260$	56.3100	0.0012	0.9830	
NIP	$y = -0.0200x + 2.7910$	16.2900	0.0200	0.6076	$y = 0.0250x + 0.4890$	37.1500	0.0013	0.9480	

**Table S2** Cd-IIP ion selection performance parameters.

Metal ion	$q$ (mg·g <sup>-1</sup> )	$K_d$ (L·g <sup>-1</sup> )	$K_{IIP}$	Metal ion	$q$ (mg·g <sup>-1</sup> )	$K_d$ (L·g <sup>-1</sup> )	$K_{IIP}$
Cd (II) Pb (II)	37.220 15.040	0.330 0.111	2.961	Cd (II) Cr (III)	26.670 6.7800	0.216 0.047	4.568
Cd (II) Cu (II)	35.920 22.320	0.315 0.175	1.801	Cd (II) Na <sup>+</sup>	22.08 20.12	0.104 0.092	1.6318
Cd (II) Ni (II)	29.970 7.880	0.250 0.055	4.503	Cd (II) NO <sub>3</sub> <sup>-</sup>	31.89 13.73	0.286 0.108	4.235